On the effect of pseudo-condensation on the design and performance of supercritical CO_2 gas chillers

Peeters, J. W.R.

DOI
10.1016/j.ijheatmasstransfer.2021.122441

Publication date
2022

Document Version
Final published version

Published in
International Journal of Heat and Mass Transfer

International Journal of Heat and Mass Transfer 186 (2022) 122441

Contents lists available at ScienceDirect

International Journal of Heat and Mass Transfer

journal homepage: www.elsevier.com/locate/hmt

On the effect of pseudo-condensation on the design and performance of supercritical CO_2 gas chillers

J.W.R. Peeters

Process and Energy, Mechanical, Maritime and Materials Engineering, Delft University of Technology, Netherlands

ARTICLE INFO

Article history:
Received 4 October 2021
Revised 5 December 2021
Accepted 15 December 2021

ABSTRACT

Supercritical CO_2 is used as a work fluid in both heat pump and power cycles. As a fluid at supercritical pressure is heated or cooled, it may undergo a smooth transition from a liquid-like state to a gas-like state or vice versa. This transition, during which the thermophysical properties vary sharply with temperature, can be referred to as pseudo- boiling or condensation. Using both analytical and numerical methods, it is shown that pseudoboiling theory helps to understand how the unique heat transfer characteristics of a supercritical fluid affect heat exchanger performance and design, in particular a gas chiller. Due to pseudo-condensation, classical approaches such as the $\varepsilon - NTU$ and LMTD methods fail when rating or designing a sCO_2 gas chiller. Using the heat of pseudo-condensation, the heat exchanger can be regarded to consist of a pre-cooler, condenser and a super-cooler. By further dividing the pre-cooler and super-cooler into two parts and subsequently applying the $\varepsilon - NTU$ method per part yields very good results with respect to both the prediction of required size and entropy generation for various operating parameters. The influence of pseudo-condensation is reduced at higher pressures and is negligible when the structural energy required for the transition from liquid-like to a gas-like state is smaller than the required thermal energy required. It is shown that the local effectiveness of the condenser part is reduced (more so than the other parts) when the heat capacity ratio R_C is varied from unity to less than unity, leading to enhanced irreversibility due to pseudo-condensation. Furthermore, the enhanced and deteriorated heat transfer regime (such as when a sCO_2 downward flow is cooled) lead to significantly different required heat exchanger sizes. Finally, through the use of Monte Carlo simulations, it shown that the uncertainty of a Nusselt correlation complicates designing heat exchangers in which pseudo-condensation occurs. The simulations show that heat exchangers should be 50% larger than the size that is predicted using a Nusselt correlation if the design performance is to be ensured.

1. Introduction

Since 1990, global warming has prompted the steady cessation of refrigerants with high global warming potential in refrigeration & heat pump cycles. Instead, supercritical carbon dioxide (sCO_2) refrigeration cycles have been developed, because CO_2 has negligible impact on the climate when compared to other refrigerants such as R134a or R22. In a conventional heat pump cycle, all processes (i.e. compression, condensation, expansion and evaporation) occur at sub-critical pressure. In contrast, in a transcritical heat pump cycle, the condensation process is at supercritical pressure, as indicated in Fig. 1a.

Global warming has also prompted the development of the supercritical and transcritical CO_2 Brayton cycle. In such a cycle, the pressure of all processes (i.e. compression, heating, expansion, cooling) is above the critical pressure, see Fig. 1b. The advantages of a sCO_2 cycle are high thermal efficiency, small equipment size (due to high fluid density), low critical temperature which may result in the avoidance of a pinch point, and a reduction in the required number of turbine stages due to the low pressure ratio, according to Liu et al. [34]. Supercritical Brayton cycles can be used with different thermal energy sources, such as coal combustion (Mecheri and Moullec [39]), geothermal energy (Ruiz-Casanova et al. [49]), waste heat (Marchionni et al. [37]) solar energy (Iverson et al. [18]), nuclear energy (Liu et al. [33]) and, in the future, possibly even fusion energy (Halimi and Suh [13]). Besides Brayton cycles, supercritical CO_2 is also considered as work fluid in organic Rankine cycles, see for instance Zhang et al. [65].

The major commonalities between the aforementioned applications are the heating and cooling processes at supercritical pressure. However, the design of these processes is challenging as

E-mail address: j.w.r.peeters@tudelft.nl

https://doi.org/10.1016/j.ijheatmasstransfer.2021.122441

List of Symbols

Greek Symbols

β	isotropic expansion coefficient in [1/K]
$\Delta\varepsilon_{95\%}$	effectiveness 95% confidence interval
μ	dynamic viscosity in [Pa.s]
ν	kinematic viscosity in [m^2/s]
ρ	density [kg/m^3]
υ	specific volume in [m^3/kg]
ε	heat exchanger effectiveness

Roman Symbols

Δh_{pb}	heat of pseudoboiling in [J/kg]
ΔT_c	temperature difference on the cold side $\left(\equiv T_{c,in} - T_{c,out}\right)$ in [K]
ΔT_h	temperature difference on the hot side $\left(\equiv T_{h,in} - T_{h,out}\right)$ in [K]
$\dot{m}$	mass flow rate [kg/s]
$\dot{Q}$	Heat load in [W]
$\dot{S}_{gen}$	rate of entropy generation in [J/K.s]
$\overline{C}$	average heat capacity rate $\equiv \dot{m}\left(\frac{h_2-h_1}{T_2-T_1}\right)$ in [J/K.s]
A	cross-sectional area in [m^2]
C	heat capacity rate, defined as $\dot{m}c_p$ in [J/K.s]
c_p	specific heat capacity at constant pressure in [J/kg.K]
C_{min}	$(\equiv \min\{C_h, C_c\})$ in [J/K.s]
D or d	diameter in [m]
h	specific enthalpy in [J/kg]
HTC	heat transfer coefficient in [W/m^2.K]
k	thermal conductivity in [W/m.K]
L	length in [m]
P	Perimeter in [m]
p	pressure in [Pa]
s	specific entropy [J/kg.K]
T	temperature in [K]
U	overall heat transfer coefficient in [W/m^2.K]
x	location in [m]

Superscripts

+	marks the lower limit of the pseudoboiling range
-	marks the upper limit of the pseudoboiling range
IG	ideal gas

Subscripts

b	bulk
c	cold side of the heat exchanger
cor	correlation
cr	critical point
exp	experimental
FC	forced convection
h	hot side of the heat exchanger
hy	hydraulic
i	partition index
in	inlet
$inner$	inner diameter
out	outlet
$outer$	outer diameter
pb	pseudoboiling
pc	psuedo-critical
ref	reference
tot	total
w	wall
GL	gas-like
LL	liquid-like

Non-dimensional numbers

B_1	ratio of structural energy to thermal energy required $\left(\equiv \frac{\Delta h_{pb/(T^+-T^-)}}{c_{p,LL}} - 1\right)$
e	error
E_q	relative work of expansion $\left(\equiv \frac{pd\upsilon}{dq}\right)$
Gr_b	Grashof number $\left(\equiv \frac{g\beta q D_h y^4}{k\nu^2}\right)$
N_{s1}	Non-dimensional entropy generation number $\left(\equiv T_{c,in}\dot{S}_{gen}/\dot{Q}\right)$
NTU	Number of transfer units
Nu_b	Nusselt number $\left(\equiv \frac{HTC\times D_h}{\lambda}\right)$
Pr_b	Prandtl number $\left(\equiv \frac{\mu c_p}{\lambda}\right)$
R_c	heat capacity rate ratio $(\equiv \min\{C_h, C_c\}/\max\{C_h, C_c\})$
Re_b	Reynolds number $\left(\equiv \frac{GD_h}{\mu_b}\right)$

a result of a phenomenon that is known as pseudo- boiling or condensation. Pseudo-boiling refers to a smooth transition from a liquid-like state to a gas like state (and vice versa for pseudo-condensation). During this transition, the thermophysical properties change considerably, giving rise to complex transport phenomena. Density variations give rise to thermal acceleration and/or buoyancy effects which in turn can either suppress or intensify turbulence, see Jackson et al. [20], Petukhov and Polyakov [45], leading to either enhanced or deteriorated heat transfer. The physics regarding the effect of thermophysical property variations on fluid flow and heat transfer is still an active field of research, see for instance Chu and Laurien [5], He et al. [14,15], Jackson [19], Peeters et al. [42,43], Peeters and Rohde [44], Ren et al. [47]. Consequently, it is not surprising that Nusselt number correlations specifically tailored for supercritical fluids include the variability of the thermophysical properties in one form or another (Ehsan et al. [6], Pioro et al. [46], Yoo [62]). Even so, predicting heat transfer to fluids at supercritical pressure at relatively simple conditions has proven to be difficult as Nusselt number correlations are (much) less accurate than their relations that were developed for sub-critical conditions. However, predicting the overall heat transfer coefficients during pseudoboiling accurately is incredibly important, not only when designing heat exchangers for refrigeration, Brayton or Rankine cycles, but also when optimizing novel cycles such as those proposed by Schöffer et al. [54], Wang and He [59].

Knowing what the effect of pseudoboiling is on heat exchanger performance is highly relevant to both Brayton and heat pump cycles. Different studies by Kauf [24], Liao et al. [32], Sarkar et al. [53], Song and Cao [57], Sánchez et al. [58], Zhang et al. [64] found that the highest coefficient of performance is found when the pressure approaches the critical pressure and when the gas cooler outlet temperature is close to or lower than the pseudo-critical temperature. In fact, the effectiveness of the gas chiller directly affects the coefficient of performance (COP) of the cycle; if the effectiveness is reduced, the COP is dimished as well. Similarly, Saeed et al. [50] found that heat exchanger effectiveness significantly influences the thermodynamic efficiency of a Brayton cycle.

The phenomenon of pseudoboiling has a direct effect on heat exchanger design; either directly through the variation of the specific heat capacity c_p or indirectly by influencing the heat transfer coefficient. Using CFD simulations, van der Kraan et al. [25] showed that for sCO_2 at pressures of below 120 bar, variable thermophysical property variations and buoyancy effects have to be taken into account when estimating the heat transfer coefficient. After performing experimental analysis on a plate exchanger Forooghi and Hooman [8] reported that the effect of wall-to-bulk thermophysical property ratios and buoyancy affect heat transfer. The former

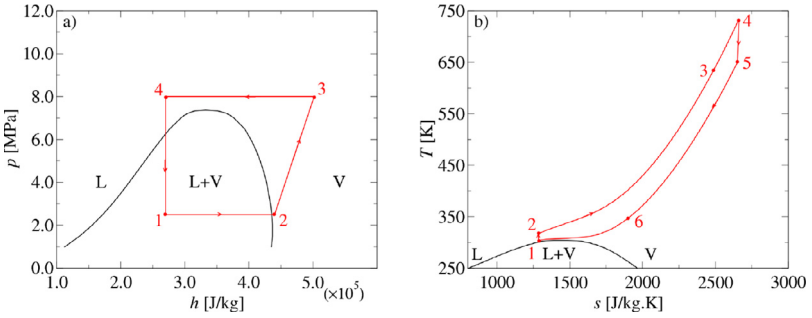

Fig. 1. a) a sCO_2 heat pump cycle, $1 \rightarrow 2$ boiler, $2 \rightarrow 3$ compressor, $3 \rightarrow 4$ condenser, $4 \rightarrow 1$ expander. b): A transcritical CO_2 Brayton cycle, $1 \rightarrow 2$ compressor, $2 \rightarrow 3$ recuperator (high pressure side), $3 \rightarrow 4$ gas heater, $4 \rightarrow 5$ turbine, $5 \rightarrow 6$ recuperator (low pressure side), $6 \rightarrow 1$ gas chiller.

was found to be more significant than the latter, especially when corrugated surfaces were used. After performing experiments with a printed circuit heat exchanger, Kruizinga et al. [27] showed that using existing Nusselt number correlations for supercritical fluids are unlikely to yield satisfactory heat transfer predictions for a heat exchanger. Li et al. [31] attempted to compensate for the Jensen inequality, see Nemati et al. [40], by introducing a novel PDF-based modelling of the average thermophysical quantities in order to enhance heat transfer predictions for printed circuit heat exchangers. Even though the previously mentioned research clearly indicates that variable thermophysical properties affect design and performance, not all researchers include the effects of variable properties in novel Nusselt number correlations for heat exchangers; see for instance Nikitin et al. [41] and Kwon et al. [30].

In this work, the relation between variable thermophysical properties and complex heat transfer characterstics of sCO_2 on heat exchanger design and performance is investigated. In particular, a gas chiller is investigated as the operating pressure of such heat exchangers is close to the critical point for both heat pump and Brayton cycles (see Wright et al. [60]). To determine the performance of the required heat transfer length, the $\varepsilon - NTU$ method is used. In this method, performance is determined in the form of effectiveness, which is defined as the ratio of the actual heat transfer rate to theoretical maximum heat transfer rate. The effectivenes can be readily determined if the number of transfer units NTU – a measure of non-dimensional heat transfer area – is known, or vice versa (see also Hesselgreaves et al. [16], Roetzel et al. [48], Zhang [63]). This method is combined with pseudoboiling theory (Banuti [1], Maxim et al. [38]) to gain better insight into the effect of pseudo- condensation. Furthermore, the role of the uncertainty that is inherent to Nusselt number correlations is discussed as well.

This paper is organised as follows; in Section 2, pseudoboiling theory is briefly summarized insofar it is relevant to the subsequent parts of the paper. In sections 3 & 4, it is shown how pseudoboiling can be accounted for in heat exchanger design. In Section 5, the effect of variations in inlet temperature and pressure on effectiveness are discussed, while in Section 6 the effect of pseudoboiling on irreversibility is investigated. Finally, in sections 7 & 8, the effect of heat transfer deterioration and uncertainty on heat exchanger performance and design is reported.

2. Definition of pseudoboiling

If the temperature of a liquid becomes equal to the saturation temperature during a heating process at sub-critical pressure, the liquid will evaporate. At the boiling point, the specific heat capacity diverges. In contrast, when a fluid at supercritical pressure is heated, a smooth transition from liquid-like behaviour to gas-like behaviour occurs that is known as pseudoboiling (Banuti [1]) or a pseudo- phase change (Kurganov et al. [28]), see Fig. 2a. During this transition the specific heat capacity shows a bell-like shape. The temperature for which the heat capacity is at its highest is denoted as the pseudo-critical temperature T_{pc}.

Kurganov et al. [28] argued that when the pseudo- phase change occurs as a result of adding heat to a fluid at (constant) supercritical pressure, a considerable change in the relative work of expansion $E_q = (pdV)/(dq)_p = p\beta/(\rho c_p)$ is observed. In the liquid-like state, i.e. when $T << T_{pc}$, $E_q \propto 10^{-2}$. In the gas-like state, or when $T >> T_{pc}$, E_q is typically $0.2 - 0.4$. Consequently, the region of the liquid-like state is determined from the condition $E_q < 0.02 - 0.03$, while the condition $E_q \approx E_q^{IG} = R/c_p^{IG}$ denotes the gas-like state.

On the other hand, Banuti [1] defined T^- and T^+ to be the start and end point of the pseudoboiling region, where $T^- << T_{pc} << T^+$. To determine the temperature interval $T^- \rightarrow T^+$, a set of linearised functions for the enthalpy in the liquid like, pseudoboiling and gas-like region, denoted as h_{LL}, h_{pb} and h_{GL}, are derived as:

$$\begin{aligned} h_{LL}(T) &= c_{p,LL}\left(T - T_{LL,ref}\right) + h\left(T_{LL,ref}\right) \\ h_{pb}(T) &= c_{p,pc}(T - T_{pc}) + h(T_{pc}) \\ h_{GL}(T) &= c_{p,GL}\left(T - T_{GL,ref}\right) + h\left(T_{GL,ref}\right) \end{aligned} \tag{1}$$

Please note that h_{LL}, h_{pb} and h_{GL} are presented here in a slightly revised form as the reference temperatures and enthalpies for the liquid-like and gas-like states are explicitly included, i.e. $T_{LL,ref}$, T_{pc}, $T_{GL,ref}$. Consulting Fig. 2b, the start and end point for the pseudo-phase change can be formulated as:

$$T^- = \frac{h_{pb} - c_{p,pb}T_{pb} - \left(h_{LL,ref} - c_{p,LL}T_{LL,ref}\right)}{c_{p,LL} - c_{p,pb}} \tag{2}$$

$$T^+ = \frac{h_{pb} - c_{p,pb}T_{pb} - \left(h_{GL,ref} - c_{p,GL}T_{GL,ref}\right)}{c_{p,GL} - c_{p,pb}} \tag{3}$$

The energy required to transition from a liquid-like state to a gas-like state at constant pressure is given as:

$$\Delta h_{pb} = \int_{T^-}^{T^+} c_p(T)dT = h\left(T^+\right) - h\left(T^-\right) \tag{4}$$

Following Maxim et al. [38], the reference states are chosen as $T_{LL,ref} = 0.5T_{pc}$ and $T_{GL,ref} = T_{cr}$. These reference temperatures correspond well to the arguments by Kurganov et al. [28], since $E_q(T^-) = 0.08$ and $E_q(T^+) = 0.22$ for sCO_2 at 8 MPa, which indicates that the CO_2 at this pressure is in a (compressed) liquid-like state when $T < T^-$, and in a gas like state when $T > T^+$. The heat of pseudoboiling Δh_{pb} for CO_2 is shown as a function of the pressure together with the heat of evaporation (at sub-critical pressures) in Fig. 2c. This figure suggests that the concept of pseudoboiling can be used alongside classical thermal-engineering ter-

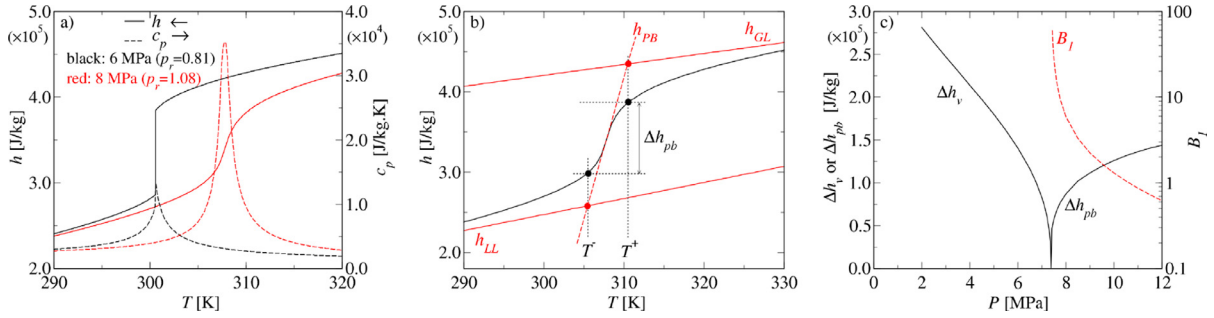

Fig. 2. a) Specific heat capacity and enthalpy for CO_2 at 6 MPa and 8 MPa. b) Definition of the heat of pseudoboiling Δh_{pb} for sCO_2 at 8 MPa. c) Heat of evaporation and heat of pseudoboiling for CO_2 as a function of the pressure. The parameter B_1 is shown as well.

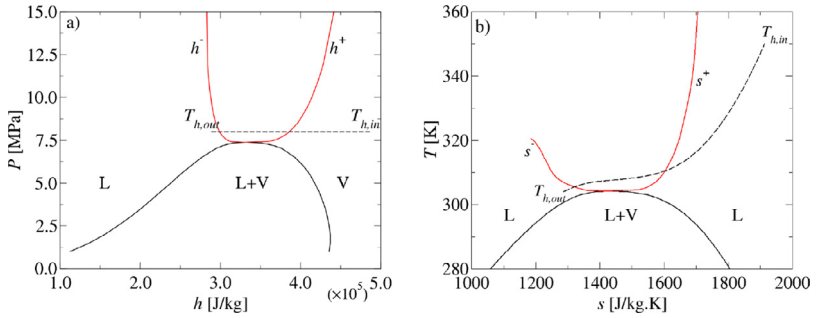

Fig. 3. A cooling process (indicated by the dashed line starting at $T_{h,in}$ and ending at $T_{h,out}$) at supercritical pressure shown in two phase diagrams: a) $P-h$ diagram, b) $T-s$ diagram. The cooling process shown here corresponds qualitatively to the process shown $3 \rightarrow 4$ in Fig. 1a or process $6 \rightarrow 1$ in Fig. 1b.

Table 1
Parameters of the theoretical heat exchanger under consideration.

m_c[kg/s]	m_h[kg/s]	$T_{h,in}$ [K]	$T_{c,in}$ [K]	U [W/m^{2}K]	P [m]	L [m]	A [m^2]
0.208	0.1	350	285	3000	0.145	3.0	0.435

minology used in heat exchanger designs, i.e. economiser heating ($h < h(T^-)$), steam generation ($h(T^-) < h(T) < h(T^+)$) and superheating ($h > h(T^+)$), an idea that was already mentioned by Kurganov et al. [28], though without using a quantification for Δh_{pb}. Finally, Banuti [1] defined the non-dimensional number $B_1 = \Delta h_{pb}/\Delta h_L - 1$. This number can be regarded as the ratio of structural energy required to overcome molecular attraction to the thermal energy required to raise the fluid temperature. Parameter B_1 is shown in Fig. 2c for CO_2. When the pressure exceeds 10.7 MPa, the structural energy required is less than the thermal energy.

The concepts and mathematical formulation of the theory outlined above are used in subsequent sections to investigate how pseudoboiling - or rather pseudo- condensation - affects gas chillers.

3. Supercritical CO_2 heat exchanger design

For both supercritical CO_2 heat pump cycles and Brayton cycles, it is feasible that the inlet and outlet temperatures of the work fluid lie outside the pseudo- condensation range. A realistic cooling process at near constant supercritical pressure is shown in a $P-h$ and a $T-s$ phase diagram in Fig. 3. In these phase diagrams, the pseudo- condensation range is indicated by either $h^- \rightarrow h^+$ or $s^- \rightarrow s^+$. It is clear that a significant part of this cooling process involves pseudo- condensation. The aforementioned cooling process can be realised by using a heat exchanger in which the CO_2 is cooled by water at an initial temperature of $T = 285$ K (for instance). First, an unbalanced heat exchanger is considered with a constant overall heat transfer coefficient – a variable heat transfer coefficient is considered in Section 7. In order to investigate how pseudo- condensation affects heat exchanger design, an unbalanced heat exchanger with the parameters listed in Table 1 is considered.

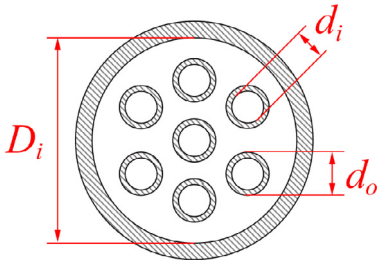

Fig. 4. Schematic of the heat exchanger geometry.

The cold source is assumed to be water with $c_p = 4180$ J/kg.K and the pressure of the CO_2 is 8 [MPa]. Furthermore, the heat exchanger geometry is reminescent of the condenser that was also used by Sánchez et al. [58]. The geometry is shown in Fig. 4. For this geometry, $d_i = 5$ [mm], $d_o = 6.6$ [mm] and $D_i = 25.4$ [mm].

For this particular heat exchanger, the transport equation for heat can be written as:

$$C_h \frac{dT_h}{dx} - \frac{d}{dx}\left(k\frac{dT_h}{dx}\right) - UP(T_h - T_c) = 0 \tag{5}$$

$$C_c \frac{dT_c}{dx} - \frac{d}{dx}\left(k\frac{dT_c}{dx}\right) - UP(T_h - T_c) = 0. \tag{6}$$

To find the temperature profiles (and thus the outlet temperatures $T_{c,out}$ and $T_{h,out}$), Eqs. (5) & (6) are solved using a Gauss-Seidel iterative method, which is described (and validated) in the appendix.

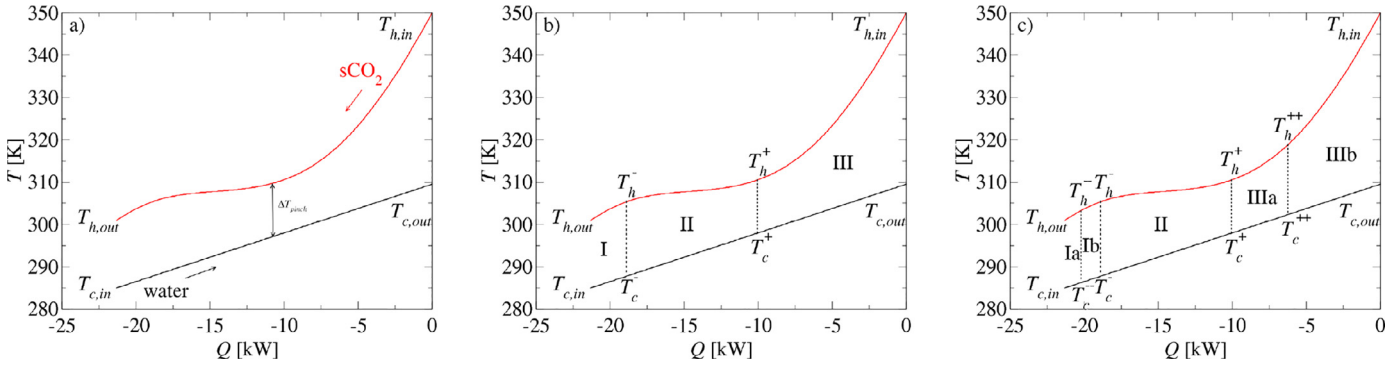

Fig. 5. A $T-Q$ diagram of the heat exchanger with sCO_2 on the hot side and water as a cold source. b) The heat exchanger is further divided into three partitions. c) Partitions I and III are divided into Ia, Ib, IIIa and IIIb.

The solution for T_h and T_c is shown in Fig. 5a. The average heat capacity of the CO_2 is easily determined as:

$$\overline{C_H} = \frac{\dot{m}_h}{T_{h,out} - T_{h,in}} \int_{T_{h,in}}^{T_{h,out}} c_{p,h} dT = \dot{m}_h \left(\frac{h_{h,out} - h_{h,in}}{T_{h,out} - T_{h,in}} \right), \tag{7}$$

which leads to the effectiveness being defined as:

$$\varepsilon = \left(\frac{\overline{C_H}}{C_{min}} \right) \frac{T_{h,in} - T_{h,out}}{T_{h,in} - T_{c,in}}. \tag{8}$$

Please note that this definition is different from the one employed by Gkountas et al. [9], as they investigated a recuperator in which the fluids on the hot and cold side are the same. From the numerical results, it is found that $T_{h,out} = 300.3$ [K] and $T_c = 309.8$ [K]. Then, according to Eq. (8), the effectiveness of this heat exchanger is equal 0.76. At this point, the combination of the numerical solutions to Eqs. (6) and (8) is little more than rating the heat exchanger in an elaborate way. The inverse problem, i.e. finding the required heat transfer area or length to obtain a desired effectiveness (or temperature difference $T_{h,in} - T_{h,out}$), is actually more relevant to heat exchanger design.

If the mass flow rates are known a-priori and the thermal load (or rather $T_{h,in}$ and $T_{h,out}$) and $T_{c,in}$ are design requirements, the thermal balance for the heat exchanger reads:

$$\dot{m}\left(h_{h,in} - h_{h,out}\right) = \overline{C_h}\left(T_{h,out} - T_{h,in}\right) = C_c(T_{c,out} - T_{c,in}) \tag{9}$$

From Eq. (9), $T_{c,out}$ is easily determined and subsequently, the effectiveness can be determined as well using Eq. (8). For a simple heat exchanger with constant fluid properties the well-known $\varepsilon - NTU$ method can be used to determine the required heat exchange area. For such a heat exchanger, the required heat transfer length can be calculated using

$$L = \frac{C_{min}}{UP(1 - R_C)} \ln\left\{ \frac{1 - \varepsilon R_C}{1 - \varepsilon} \right\}, \tag{10}$$

where the ratio of heat capacities is defined as

$$R_C = \frac{C_{min}}{C_{max}} \tag{11}$$

in which $C_{\min} = \min\left\{\overline{C_H}, C_C\right\}$ and $C_{\max} = \max\left\{\overline{C_H}, C_C\right\}$. For the heat exchanger described above, $R_C = 0.5$. Consequently, Eq. (10) yields a required heat transfer length of $L = 1.9$ [m], which is considerably smaller than the length indicated in Table 1.

The discrepancy stems directly from the fact that dT_h/dx is not at all constant over the length of the heat exchanger; a direct result of the pseudo- condensation phenomenon. To solve this problem, researchers have devised different solutions, such as modifying the log mean temperature difference by introducing an empirical correction factor (see Kwon et al. [29]) or by dividing the heat exchangers into many sub-exchangers and applying the $\varepsilon - NTU$ method for each sub-exchanger (see Gkountas et al. [9], Guo [11] and Jiang et al. [22,23]).

Looking at the solution for T_h and T_c in Fig. 5a, it is tempting to divide the heat exchanger into three separate partitions (see Fig. 5b) - a stategy that is also used when dealing with sub-critical phase changes in heat exchangers, i.e. boilers and condensers, see for instance Luyben [35]. The definitions of the partitions are as follows: partition I) – The sCO_2 is in the liquid-like state ($T_h < T^-$), partition II) – the sCO_2 is in a pseudo- condensing state ($T^- < T_h < T^+$), partition III) – the sCO2 is in a gas-like state ($T_h > T^+$). T_c^+ and T_c^- as indicated in Fig. 5b, are found by setting up the following thermal balances;

$$\begin{aligned} C_c\left(T_{c,out} - T_c^+\right) &= \overline{C_{h,III}}\left(T_{h,in} - T_h^+\right) \\ C_c\left(T_c^+ - T_c^-\right) &= \dot{m}\Delta h_{pb} \\ C_c\left(T_c^- - T_{c,in}\right) &= \overline{C_{h,I}}\left(T_h^- - T_{h,out}\right) \end{aligned} \tag{12}$$

Calculating $\overline{C_h}$, ε and R_C for each section individually - see Table 2b - now yields $L = 2.74$ [m], which is much closer to the required heat transfer length than the attempt in which no partitions were considererd.

The prediction can be further enhanced by also dividing partitions I and III into Ia, Ib, IIIa and IIIb, respectively, as indicated by Fig. 5c. The temperatures T_h^{++} and T_h^{--} are chosen to be equal to 318.4 K and 303 K, respectively. The temperatures T_c^{--} and T_c^{++} are found from setting up a thermal balance per partition. Following the same procedure as before now yields a required length of $L = 2.91$[m]. From Table 2c, it is clear that subdividing section I (where the sCO_2 is in a liquid-like state) into two separate parts does not enhance the prediction of the required length, as $L_I = 0.39$ [m] and $L_{Ia} + L_{Ib} = 0.38$ [m]. Rather, it is the sub-division of the third partition that leads to the improved prediction of the required length, i.e. $L_{IIIa} + L_{IIIb} = 1.17$ [m] is clearly larger than $L_{III} = 0.99$ [m]; this finding need not be a general rule of thumb, however.

Note that dividing the heat exchanger into five partitions (with each partition having an equal temperature glide) can actually result in unphysical results, especially for cases very close to the critical point. In Fig. 6, the $\varepsilon - NTU$ method is compared with and without the application of the concept of pseudo- condensation for different lengths. It is clear that without the application of pseudo-condensation concept, the $\varepsilon - NTU$ gives unsatisfactory results. After all, it is physically unrealistic that a higher effectiveness could be obtained by shortening the heat transfer length. This erroneous result can be mitigated by simply adding more partitions. However, as is indicated in Fig. 6, doubling the number of partitions still yields unrealistic results. When the concept of pseudo-boiling

Table 2
Details of the different modelling strategies indicated by Fig. 5. $C_c = 868$ J/Ks.

Partition	ΔT_h	ΔT_c	$R_{c,i}$	$C_{\min}$	$\overline{C_{h,i}}$	L_i	$\boldsymbol{L_{tot}}$
N/A	350.0–300.3	285.0–309.9	0.5	C_h	432.5	1.9	**1.90**
Partition	ΔT_h	ΔT_c	$R_{c,i}$	$C_{\min}$	$\overline{C_{h,i}}$	L_i	$\boldsymbol{L_{tot}}$
III	350.0–310.5	298.0–309.9	0.30	C_h	258	0.99	
II	305.5–305.5	298.0–288.0	0.50	C_c	1740	1.36	**2.74**
I	305.5–300.3	288.0–285.0	0.62	C_h	538	0.39	
Partition	ΔT_h	ΔT_c	$R_{c,i}$	$C_{\min}$	$\overline{C_{h,i}}$	L_i	$\boldsymbol{L_{tot}}$
IIIb	350.0–318.4	302.3–309.9	0.24	C_h	206	0.57	
IIIa	318.4–310.5	298.0–302.3	0.54	C_h	468	0.60	
II	310.5–305.5	288.0–298.0	0.50	C_c	1740	1.36	**2.91**
Ib	305.5–303.0	286.2–288.0	0.69	C_h	600	0.20	
Ia	303.0–300.3	285.0–286.2	0.45	C_h	481	0.18	

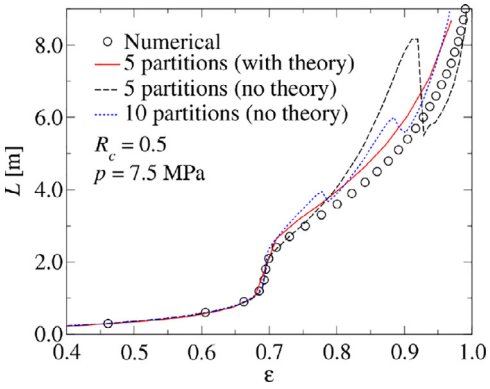

Fig. 6. Comparison of the $\varepsilon - NTU$ methods with and without the theory of pseudo-condensation.

is used, the heat capacity ratio is more accurately determined then it is without the same concept.

These results show that using the $\varepsilon - NTU$ method can be applied reliably if the heat exchanger is divided in three partitions that are defined using T^- and T^+ and by subsequently dividing the partitions in which sCO_2 has gas-like properties and liquid-like properties into two separate partitions. For even better predictions of the required heat transfer area, more partitions can be added. For the remainder of this article, only five partitions will be considered.

4. Effect of pseudo- condensation on heat transfer length

In this section, it is shown that the five partitions $\varepsilon - NTU$ method can also be used to calculate the required heat transfer length for i) different heat capacity ratio's and ii) when the outlet temperature of the sCO_2, $T_{h,out}$, is in or outside the pseudo- condensation range. The transport equations Eqs. (5) & (6) are again numerically solved, but for different heat exchanger lengths; $L = 0.3 - 9.0$ [m]. For each heat exchanger length, the $\varepsilon - NTU$ method is applied as well. The number of partitions used is determined by the value of $T_{h,out}$. Thus, referring back to Fig. 5c, five partitions are used when $T_{h,out} < T^{--}$. Four partitions are used when $T^{--} < T_{h,out} < T^-$, three are used when $T^- < T_{h,out} < T^+$, two when $T^+ < T_{h,out} < T^{++}$ and only one partition is used when $T_{h,out} >> T^{++}$.

A comparison of the required heat transfer length when using no partitions and when using five partitions is shown in Fig. 7. It is clear that for any heat exchanger length, the five partitions $\varepsilon - NTU$ method is in very good agreement with the numerical results when $R_C = 0.25 - 0.5$. When $R_C = 1.0$, the five partitions method is in good agreement with the numerical results. It is also clear that using the $\varepsilon - NTU$ method without partitioning leads to significant underpredictions of the required heat transfer length whenever pseudo- condensing occurs for all investigated R_C. For instance, when ε is required to be equal to 0.7, lack of partitioning yields $L = 1.3, 1.5, 2.3$ [m] for $R_C = 0.25, 0.5, 1.0$, which corresponds to the required lengths to be underestimated by 42%, 50%, 180%, respectively.

5. Effect of temperature and pressure on effectiveness

While the effectiveness in Fig. 7 could also be shown as a function of NTU, the result would not be universal (like the $\varepsilon - NTU$ method is for fluids with constant properties). Unlike the heat transfer length, the effectiveness of the heat exchanger is not simply the sum of the local effectiveness of the partitions ε_i:

$$\varepsilon = \sum_{i=1}^{N} \frac{C_{min,i}}{C_{min}} \left(\frac{(T_{h,in})_i - (T_{c,in})_i}{T_{h,in} - T_{c,in}} \right) \varepsilon_i, \tag{13}$$

in which N is the number of partitions and the index refers to a quantity belonging to partition i. As a result of $c_p = f(T, p)$, not only the inlet temperature, outlet temperature and pressure of the supercritical side affect the effectiveness. Due to the variation of $C_{min,i}$ along the heat exchanger length, the effectiveness also depends on the difference between the inlet temperatures per partition. In Fig. 8 the effectiveness versus the length is shown for different process conditions. In Fig. 8a, the effect of $T_{h,in}$ is shown. As the difference $T_{h,in} - T_{c,in}$ is increased (while keeping $T_{c,in}$ the same), the temperature difference at the pinch point becomes smaller when $L > 4$. Hence, when increasing $T_{h,in}$, a longer heat exchanger length is required in order to obtain the desired effectiveness. For $L << 4$, the opposite is true.

In Fig. 8b, the effectiveness versus the length is shown for different inlet temperatures $T_h = 280 - 290$ K, while keeping the inlet temperature difference $T_{h,in} - T_{c,in}$ constant. It is clear from Fig. 8 that different inlet temperatures, but the same global temperature difference, results in significantly different effectiveness. The closer $T_{c,in}$ is to the pseudo- condensation range, the smaller the temperature difference at the pinch point will be and thus the larger the required length will be.

The effect of the pressure is shown in Fig. 8c. For higher reduced pressures, the effect of pseudo- condensation on effectiveness is significantly decreased. At a pressure of 11 MPa, the effect of pseudo- condensation is no longer apparent. This result is agreement with earlier findings in literature by van der Kraan et al. [25].

While it is clear from Eq. (13) that the effectiveness depends on the process conditions, it is rather limited in its usefulness. After

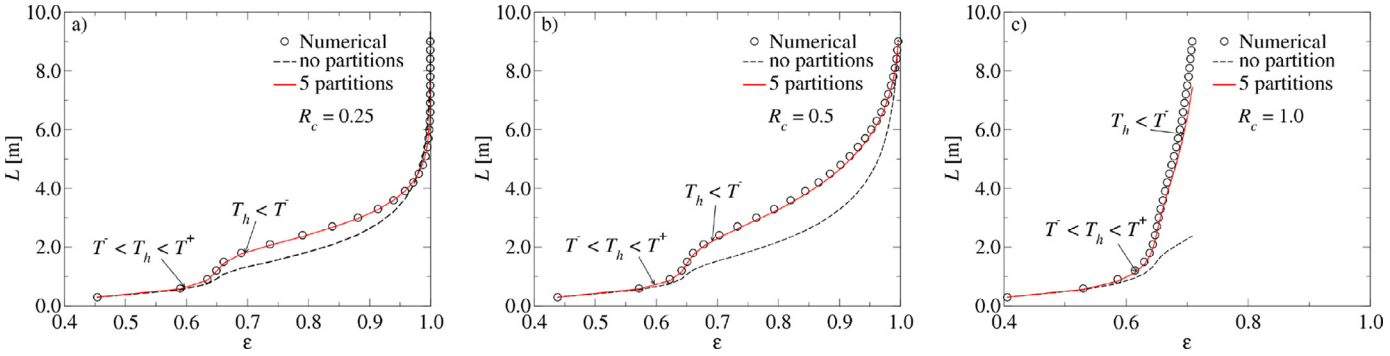

Fig. 7. Length versus effectiveness for different heat capacity ratios R_C. The minimum lengths for which the outlet temperature of the sCO_2 is between $T^- - T^+$ and for which it is lower than T^- have been indicated.

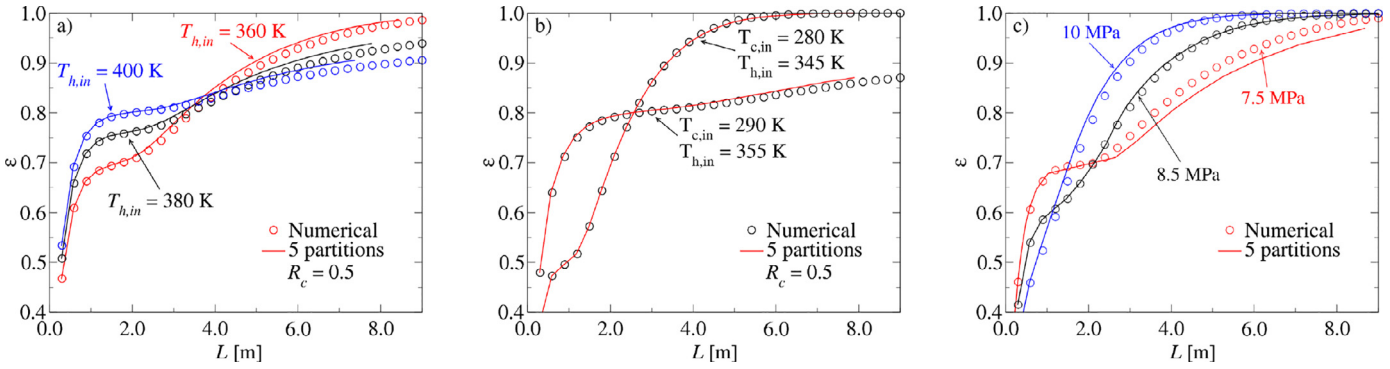

Fig. 8. Length versus effectiveness for different heat capacity ratios and different process conditions as indicated.

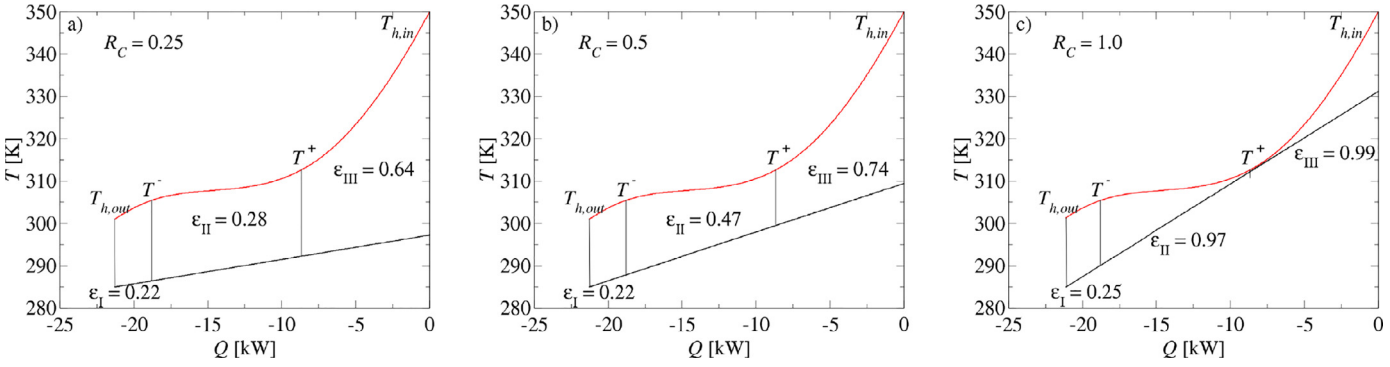

Fig. 9. Local effectiveness ε_i shown inside $T - Q$ diagrams for three heat exchangers for which R_C =0.25, 0.5 and 1.0. For all heat exchangers, the effectiveness is equal to 0.75.

all, the effectiveness ε is easily determined without the concept of local effectiveness ε_i. However, Eq. (13) is valid irrespective of the number of partitions chosen (in fact, if only one partition is used, the equation reduces to the trivial result $\varepsilon = \varepsilon$, which was defined earlier by Eq. (8)). It is convenient to think of the heat exchanger as though it consists of a pre-cooling part, a condenser and a super-cooling part. Fig. 9 shows the $T - Q$ diagrams of three different heat exchangers, for which $\varepsilon = 0.75$ and $R_C = 0.25, 0.5$ and 1.0. In these diagrams, the pre-cooling, condenser and super-cooling parts have been denoted again as III, II and I. Note that the thermal load (and thus $T_{h,in} - T_{h,out}$) is the same for all three exchangers. However, the temperature rise of the water is not the same and therefore, the local effectiveness also is not. When comparing the local effectiveness of $R_C = 1.0$ with $R_C = 0.5$ and $R_C = 0.25$ for all three parts, it becomes clear that the local effectiveness in the condenser part is the most negatively affected by imbalancing: $\varepsilon_{II} = 0.97, 0.47$ and 0.28 for $R_C = 1.0, 0.5$ and 0.25, respectively. The local effectiveness in the pre-cooler ε_{III} and super-cooler ε_I also decrease as R_C decreases, but ε_I does so only marginally. Furthermore, it is clear that as R_C is decreased, the local temperature difference $T_h(x) - T_c(x)$ becomes larger, which is a typical indicator for enhanced irreversibility. Unsurprisingly, there is a connection between irreversibility and local effectiveness, which will be discussed in the next section.

6. Effect of pseudo- condensation on irreversibility

Heat exchangers can be considerable sources of irreversibilities in thermodynamic cycles; see for instance Fartaj et al. [7], Sarkar [52]. The irreversibility is proportional to the rate of entropy gen-

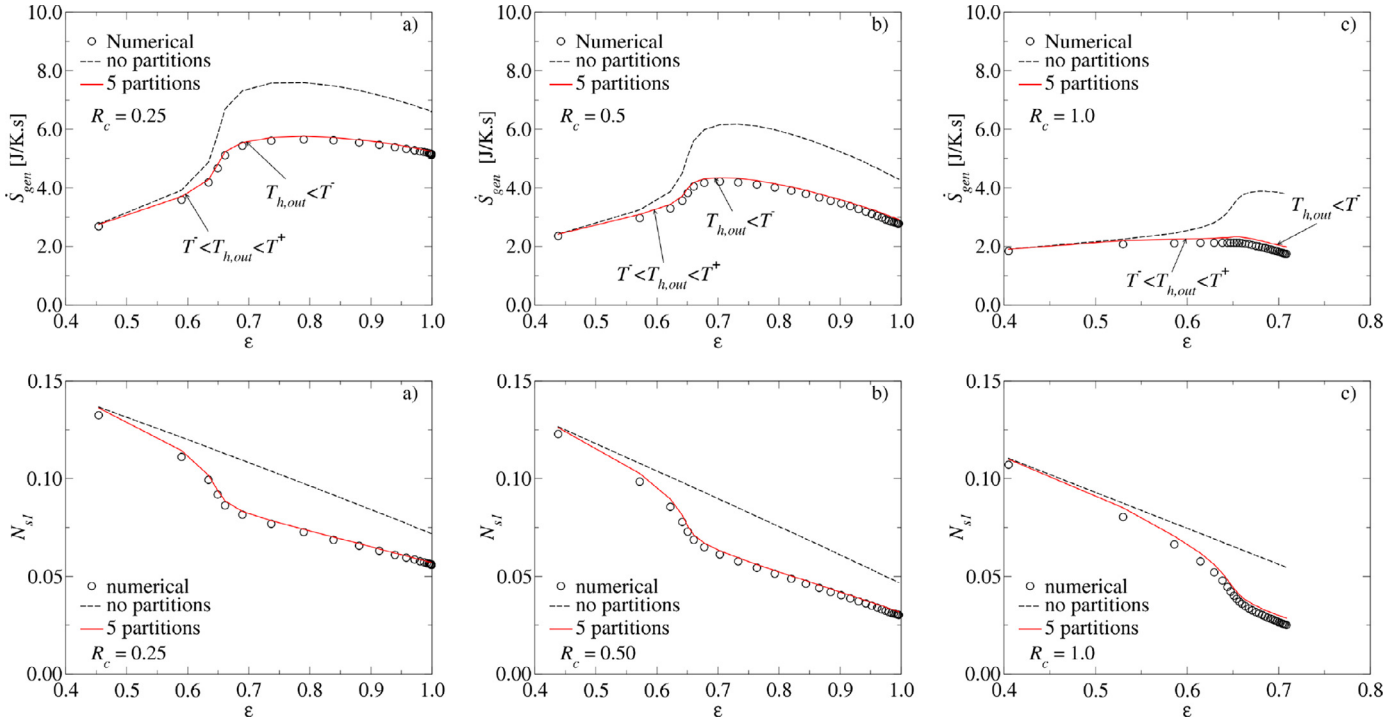

Fig. 10. Entropy generation $\dot{S}_{gen}$ (1st row) and entropy generation number N_{s1} (2nd row) versus effectiveness for different heat capacity ratios.

eration as $\dot{I} = T_{ref}\dot{S}_{gen}$, according to Manjunath and Kaushik [36], Sekulić [56] and Sciacovelli et al. [55]. Exergy is destroyed by irreversbilities associated with friction and stream to stream heat transfer. Following Bejan [2], Hesselgreaves [17], Sekulić [56], Manjunath and Kaushik [36], the rate of entropy generation of a heat exchanger in which the fluids can be considered to have constant thermophysical properties and for which frictional losses can be neglected, can be written as:

$$\dot{S}_{gen} = \overline{C_h} \ln\left\{\frac{T_{h,out}}{T_{h,in}}\right\} + C_c \ln\left\{\frac{T_{c,out}}{T_{c,in}}\right\} \tag{14}$$

Using Eq. (8), the rate of entropy generation is easily written as a function of the effectiveness:

$$\dot{S}_{gen}(\epsilon) = \overline{C_h} \ln\left\{1 - \frac{C_{min}}{\overline{C_h}}\varepsilon\left(1 - \frac{T_{c,in}}{T_{h,in}}\right)\right\} + C_c \ln\left\{1 + \frac{C_{min}}{C_c}\varepsilon\left(\frac{T_{h,in}}{T_{c,in}} - 1\right)\right\} \tag{15}$$

Following Hesselgreaves [17], the entropy generation can be written in non-dimensional form using the definition of the entropy generation number:

$$N_{s1}(\epsilon) = \left(\varepsilon\left(\frac{T_{h,in}}{T_{c,in}} - 1\right)\right)^{-1}\left[\frac{\overline{C_h}}{C_{min}} \ln\left\{1 - \frac{C_{min}}{\overline{C_h}}\varepsilon\left(1 - \frac{T_{c,in}}{T_{h,in}}\right)\right\} + \frac{C_c}{C_{min}} \ln\left\{1 + \frac{C_{min}}{C_c}\varepsilon\left(\frac{T_{h,in}}{T_{c,in}} - 1\right)\right\}\right] \tag{16}$$

Like Eq. (10), Eqs. (15) and (16) can be applied per partition in order to obtain the total rate of entropy generation by summing all contributions per partition:

$$\dot{S}_{gen} = \sum_{i}^{N} \dot{S}_{gen}(\epsilon_i). \tag{17}$$

In Fig. 10, the entropy generation rate is shown as a function of the effectiveness ($T_{c,in} = 285$ K, $T_{h,in} = 350$ K) for the heat exchanger from Section 4. It is clear that irrespective of the heat capacity ratio R_C, the entropy generation (either in dimensional or non-dimensional form) is well predicted using the $\varepsilon - NTU$ method. Without partitioning, the entropy generation is severely overpredicted when $T_{h,out} < T^+$. It is interesting to note here that pseudo- condensation results in enhanced absolute irreversibility ($\dot{S}_{gen}$), but in reduced relative irreversibility (N_{s1}), which is most clear when $R_C < 1$. In other words, when the effectiveness increases, the thermal load increases faster than the destruction of available work does. Comparing the entropy generation for different heat capacity ratios shows that the entropy generation is smallest for the balanced heat exchanger. In fact, for $R_C = 1$, pseudo- condensation does not lead to enhanced entropy generation like it does when $R_C < 1.0$. Following the analysis of the previous section, the enhancement of the entropy generation for $R_C < 1$ coincides with reduced local effectiveness in the condenser and the pre-cooler parts. However, the enhanced irreversibility is not per se the result of reduced local effectiveness. Rather, in the condenser especially, the local heat capacity ratio $R_{C,i}$ is much less than unity, which leads to the enhancement of $\dot{S}_{gen}$.

7. Variable heat transfer coefficient

In the previous analyses, it was assumed that the overall heat transfer coefficient was a constant. However, it is well known that the heat transfer coefficient of heated or cooled supercritical fluids vary as a result of the thermophysical property variation, see Ehsan et al. [6], Pioro et al. [46], Yoo [62]. At relatively low heating rates, the heat transfer coefficient typically shows a maximum close to when the bulk temperature is equal to the pseudo-critical temperature (Yamagata et al. [61]), or when $T_b < T_{pc} < T_w$ (Peeters and Rohde [44]) for heated flows. Depending on flow conditions (laminar or turbulent), flow orientation, as well as heating or cooling conditions, heat transfer to supercritical fluids can be enhanced or deteriorated. Enhancement typically occurs in upward cooled flows, or in heated downward flows, while heat transfer deterioration may occur in heated upward flows or cooled downward flows. Deterioration typically occurs when turbulent motions are supressed and

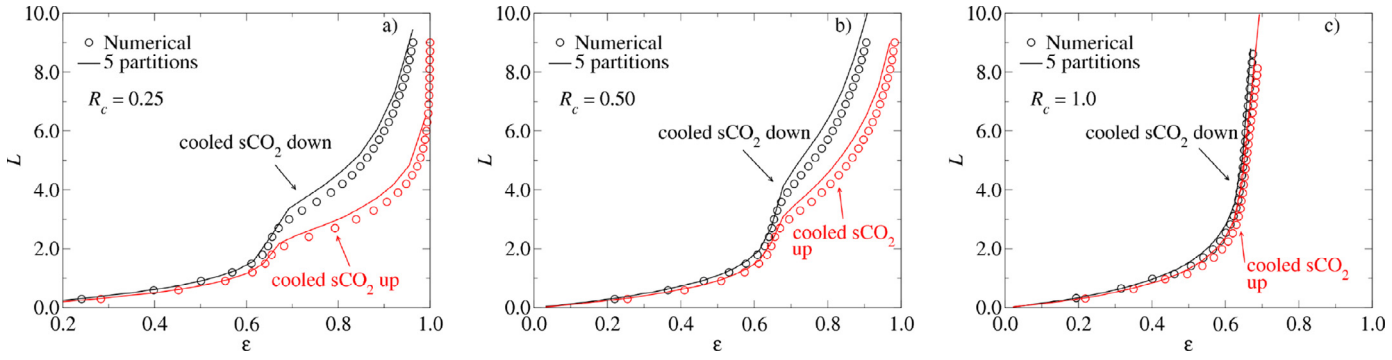

Fig. 11. Length versus effectiveness for different heat capacity ratios for upward flowing cooled sCO$_2$ (enhanced heat transfer) and downward flowing cooled sCO$_2$ (deteriorated heat transfer).

the flow laminarizes, the cause of which are non-negligible buoyancy forces and/or bulk acceleration. The difference between enhanced and deteriorated heat transfer can be large enough to potentially influence heat exchanger design.

To investigate the latter statement, the same heat exchanger is considered as before, except that *UP* in Eq. (6) is now calculated as:

$$UP = \left(\frac{1}{\pi HTC_h d_o} + \frac{1}{\pi HTC_c d_i} \right)^{-1}, \tag{18}$$

where HTC_h and HTC_c are the heat transfer coefficient of the hot and cold side, respectively. The same five partitions $\varepsilon - NTU$ method as before can be used if the average heat transfer coefficient per partition is used, i.e. $U_i = (U(T_{h,in})_i + U(T_{h,out})_i)/2$. To account for heat transfer deterioration or enhancement in cooled downward flows at supercritical pressure, the Nusselt correlation by Bruch et al. [3] is used:

$$\begin{aligned} \frac{Nu_b}{Nu_{FC}} &= 1 - 75\left(\frac{Gr}{Re_b^{2.7}}\right)^{0.46} \quad \text{when} \quad \frac{Gr}{Re_b^{2.7}} < 4.2 \cdot 10^{-5} \\ \frac{Nu_b}{Nu_{FC}} &= 13.5\left(\frac{Gr}{Re_b^{2.7}}\right)^{0.4} \quad \text{when} \quad \frac{Gr}{Re_b^{2.7}} > 4.2 \cdot 10^{-5} \end{aligned} \tag{19}$$

Eq. (19) represents heat transfer deterioration due to laminarization when $Gr/Re_b^{2.7} < 4.2 \cdot 10^{-5}$ and enhancement when $Gr/Re_b^{2.7} > 4.2 \cdot 10^{-5}$. For upward cooled sCO$_2$, the following relation applies:

$$\frac{Nu_b}{Nu_{FC}} = \left(1.542 + 3243\left(\frac{Gr}{Re_b^{2.7}}\right)^{0.91} \right)^{1/3}. \tag{20}$$

In the above relations, Nu_{FC} is the relation by Krasnoshchekov et al. [26] which was later modified by Jackson and Hall [21]:

$$Nu_{FC} = 0.0183 Re_b^{0.82} \overline{Pr}^{0.5} \left(\frac{\rho_b}{\rho_w}\right)^{-0.3}. \tag{21}$$

The previous heat exchanger calculations from Section 4 are repeated here, but this time while accounting for the variable heat transfer coefficient. The results are shown in Fig. 11. Two different observations can be made. The five partitions $\varepsilon - NTU$ method yields very reasonable predictions for different heat capacity ratios. More importantly, a different heat transfer length is required for a given effectiveness, depending on whether the sCO$_2$ flows up- or downwards. In the cases of $R_C = 0.5$ and $R_C = 0.25$, the difference in required heat transfer area is significant. This result stems from the fact that the thermal resistance of the sCO$_2$ is larger than the thermal resistance of the cold source. While these results are certainly not universal, it is clear that laminarization of the sCO$_2$ flow leads to larger heat exchanger design. Therefore, to avoid laminarization in sCO$_2$ heat exchangers, it is likely to be very economical to employ geometries that promote turbulence, such as fins, grooves or inserts.

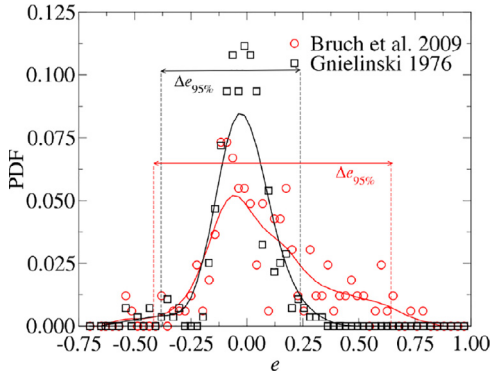

Fig. 12. Probability density function of e for the Nusselt correlation by Bruch et al. [3] (representing cooled downward flowing sCO$_2$) and Gnielinski [10] (representing heat transfer to turbulent fluids at sub-critical pressure without significant thermophysical property variations.

8. Uncertainty in heat transfer predictions

Heat transfer to fluids at supercritical pressure is notoriously difficult to predict accurately when compared to heat transfer at sub-critical pressure. To lend a modicum of credence to the latter statement, errors associated with Nusselt number correlations were investigated for both Eq. (19) and the well-known Gnielinski [10] correlation, (a correlation that is widely accepted as being accurate for single phase heat transfer at sub-critical pressure). For both correlations, the probability density function of the relative error, as well as the corresponding 95% confidence interval is investigated. The relative error of a correlation can be defined as:

$$e \equiv \frac{Nu_{exp} - Nu_{corr}}{Nu_{corr}} \tag{22}$$

A comparison of the probability density functions of e for both correlations is shown in Fig. 12. It is clear that Eq. (19) is significantly less accurate at predicting heat transfer to sCO$_2$ than the Gnielinski correlation is at predicting heat transfer to fluids at sub-critical pressure. Particularly, Eq. (19) is much more likely to yield over-predictions. This lack of accuracy can also be found amongst other correlations that were specifically developed for supercritical fluids, a fact that was recently clearly portrayed by Guo et al. [12].

This lack of accuracy is potentially undesirable when designing heat exchangers. The uncertainty accompanying the correlation means that both the effectiveness and the required heat transfer area cannot be determined accurately, which in turn may lead to over-designed heat exchangers. By performing Monte Carlo simulations the propagation of the error associated with Eq. (19) can be investigated. To this end, the inverse cumulative probability density function (inverse CDF) corresponding to the PDF of the error

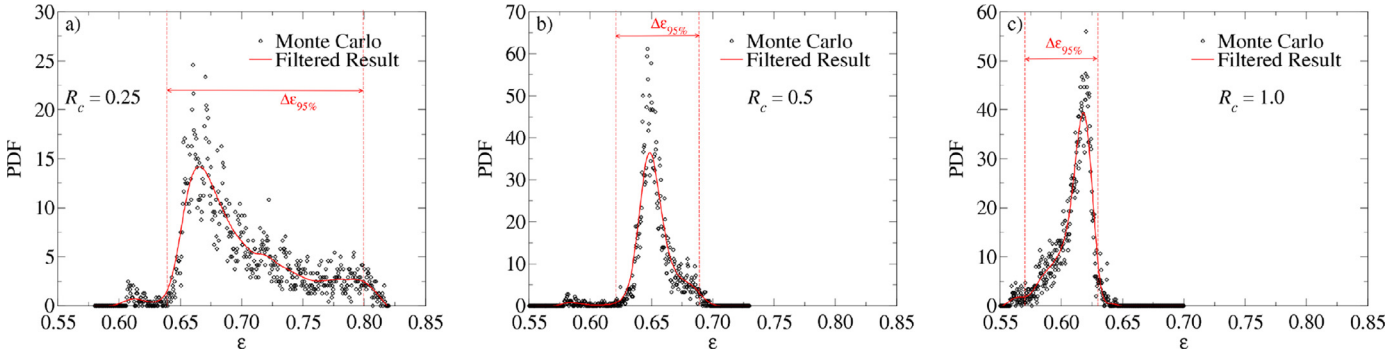

Fig. 13. Probability density functions of the effectiveness for a heat exchanger with $L = 3$ m, $T_{h,in} = 350$ K and $T_{c,in} = 285$ K. The smooth red line is the filtered result of the raw data. The dashed lines indicate the 95% confidence interval. (For interpretation of the references to colour in this figure legend, the reader is referred to the web version of this article.)

in Eq. (22), is created. A Monte Carlo simulation can then be carried out as follows:

1. a random number between 0 and 1 is generated.
2. using the random number, the error e is detemined from the inverse CDF.
3. the Nusselt number (and thus the heat transfer coefficient) is then determined from $Nu = Nu_{cor}(1 + e)$
4. the transport equations for the thermal energy are solved as described under Section 3.
5. the effectiveness is determined and recorded
6. steps 1 to 5 are repeated N times.
7. determine the PDF of the effectiveness.

This procedure was applied to the heat exchanger that was previsouly described in Section 3 for three different heat capacity ratios with $N = 5000$; see Fig. 13. It is clear that in the $R_C = 0.25$ case (or when the thermal resistance of the sCO_2 is dominant) the uncertainty of the correlation has a significant effect on the possible outcome of the effectiveness. The 95% confidence interval is $\varepsilon = 0.63 - 0.75$. For the other heat capacity ratios (for which the thermal resistance of the water is larger), the effect of the uncertainty is less clear; the 95% confidence intervals are $\varepsilon = 0.58 - 0.69$ and $0.58 - 0.64$, respectively.

While the spread of potential effectiveness outcomes may not mean much in terms of the thermal load as $Q = \varepsilon C_{\min}\left(T_{h,in} - T_{c,out}\right)$ at first, it is important to note that high thermal effectiveness is important in order to achieve high cycle efficiencies, as is outlined by Brun et al. [4], Saeed et al. [51] and Saeed et al. [50]. Therefore, it is important to know how the uncertainty accompanying any Nusselt correlation affects the size of the sCO_2 heat exchangers. The Monte Carlo method that was used before can also be used to investigate the latter. The procedure then is as follows:

1. steps 1, 2 and 3 of the previous Monte Carlo simulation are repeated
4. using the five partitions $\varepsilon - NTU$ method, the required length is determined and recorded
5. steps 1 to 4 are repeated for N times
6. the PDF of the required length is determined
7. the 95% confidence interval is determined for the required length

The results of the latter procedure are shown in Fig. 14. The Nusselt correlation has a significant effect on the required heat exchanger size for both balanced and unbalanced heat exchangers. For the investigated heat capacity ratios, the upper bound of the 95% confidence interval is 42%, 39% and 42% larger than what is predicted by the Nusselt correlation for $R_C = 0.25, 0.5$ and 1.0, respectively. These results mean that any heat exchanger design should be at least over 42% larger than what is predicted by the Nusselt correlation, in order to ensure that the heat exchanger performs as intended. This is even true for the balanced heat exchanger, where the thermal resistance of the supercritical fluid has less influence than in the other cases.

9. Conclusions

In this paper, the effect of pseudo- condensation at supercritical pressure on the design of gas chillers is investigated. By combining the classical $\varepsilon - NTU$ method with pseudoboiling theory, the gas chiller can be regarded as the combination of a pre-cooler, a condenser and a super-cooler. To predict the required size of the heat

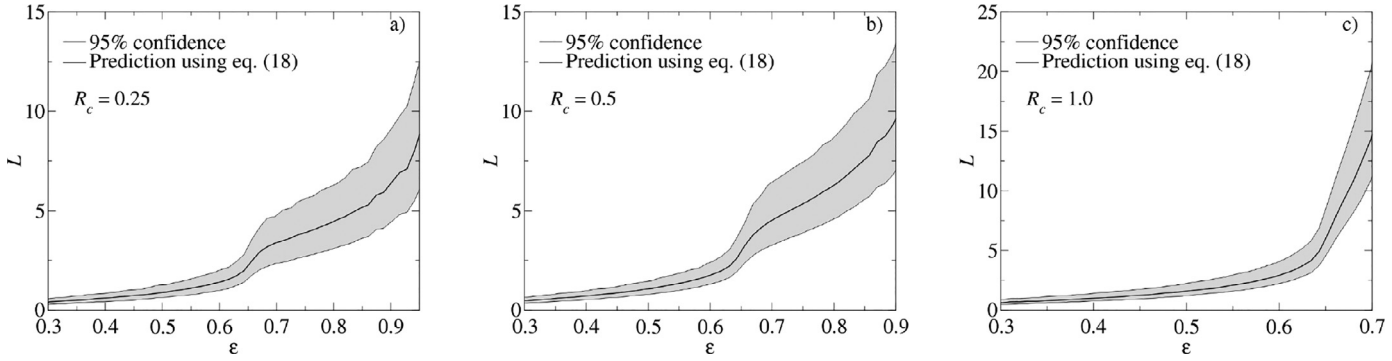

Fig. 14. Length versus effectiveness with 95% confidence bands.

exchanger, the pre-cooler and super-cooler should be divided into two separate parts. This method was used to show how pseudo-condensation affects gas chillers at supercritical pressure.

As a result of pseudo-condensation, the effectiveness of the gas chiller depends not only on the heat capacity ratio and the heated length, but also on inlet temperatures and operating pressure. Furthermore, when the heat capacity ratio changes from unity to less than unity, the local effectiveness of the condenser partition is significantly reduced. A decrease in local effectiveness as a result of imbalancing coincides with enhanced entropy generation as a result of pseudo- condensation. Thus, when operating conditions vary from design specifications, the effectiveness varies signifcantly as well, which may impact the thermal efficiency or COP in supercritical power- and heat pump cycles.

Heat transfer deterioration can affect the required size significantly. In the examples discussed in this work, the maximum difference between required lengths in enhanced and deteriorated heat transfer regime was characterised by a factor larger than two. This result highlights the need for heat transfer enhancement when operating in the deteriorated heat transfer regime.

As a result of the large uncertainties that accompany Nusselt correlations (especially for the deteriorated heat transfer regime), gas chillers may not perform as intended. Through Monte Carlo simulations, it was shown that the effectiveness shows significant variations as a result of Nusselt number uncertainty when the heated length was kept constant. Vice versa, the Nusselt number uncertainty leads to significant uncertainty in the required heat transfer length; heat exchangers involving sCO_2 may well need to be over 50% larger in reality than a design that is based on Nusselt number correlations.

Finally, it should be noted that the conclusions regarding the variability and uncertainty of heat transfer coefficients need not be valid for each and every heat exchanger involving sCO_2. However, the corresponging results, analyses and conclusions serve as an indicator to other designs if similar conditions are applicable.

Declaration of Competing Interest

The authors declare that they have no known competing financial interests or personal relationships that could have appeared to influence the work reported in this paper.

Appendix A. Numerical model

In discrete form, the thermal energy balance on the hot side of the heat exchanger can be written as:

$$\dot{Q}|_{i+1/2} - \dot{Q}|_{i-1/2} - UP\Delta x(T_h|_i - T_c|_i) = 0, \tag{A.1}$$

where $\dot{Q} = \dot{m}_h h_h - kA(dT/dx)$. The thermal gradients can be approximated as $dT_h/dx|_{i+1/2} \approx -k_p(T_h|_{i+1} - T_h|_i)/dx$ and $dT_h/dx|_{i-1/2} \approx -k_m(T_h|_i - T_h|_{i-1})/dx$, where $k_p = 1/2(k|_{i+1} + k|_i)$ and $k_m = 1/2(k|_i + k|_{i-1})$. Dividing by Δx yields:

$$\begin{aligned}&\dot{m}_h\left(\frac{h_h|_{i+1/2} - h_h|_{i-1/2}}{\Delta x}\right)\\ &-\frac{A}{\Delta x^2}(k_pT_h|_{i+1} - (k_p + k_m)T_h|_i + k_mT_h|_{i-1})\\ &-UP\Delta x(T_h|_i - T_c|_i) = 0\end{aligned} \tag{A.2}$$

Since $dh = c_p dT + (1 - \beta T)dp/\rho \approx c_p dT$, the convective term can be rewritten as:

$$\dot{m}_h\left(\frac{h_h|_{i+1/2} - h_h|_{i-1/2})}{\Delta x}\right) \approx C_h\left(\frac{T_h|_{i+1/2} - T_h|_{i-1/2}}{\Delta x}\right). \tag{A.3}$$

Finally, noting that $T_h|_{i+1/2} \approx 1/2(T_h|_{i+1} + T_h|_i)$, an explicit expression for $T_h|_i$ is obtained:

$$\begin{aligned}T_h|_i = &\left(\frac{1}{\frac{A(k_m+k_p)}{\Delta x^2} + UP}\right)\left(UPT_c|_i + \left(\frac{Ak_m}{\Delta x^2} - \frac{C_h}{\Delta x}\right)T_h|_{i-1}\right.\\ &\left.+\left(\frac{Ak_p}{\Delta x^2} + \frac{C_h}{\Delta x}\right)T_h|_{i+1}\right)\end{aligned} \tag{A.4}$$

Eq. (A.4) is iteratively used in conjunction with similar expression for $T_c|_i$, until a converged solution is found. Every 200 iterations, a Savitsky-Golay filter is applied to ensure that a converged solution can be found.

Appendix B. model validation

Consider a heat exchanger consisting of three parts; a pre-heater, an evaporator and a super heater. A supercritical fluid is heated by a hot gas for which $C_h = 465$ J/K.s. For the supercritical fluid, the following is true;

$$c_p = \begin{cases} c_{p,LL} & T < T^- \\ \frac{\Delta h_{pb}}{T^+ - T^-} & T^- < T < T^+ \\ c_{p,GL} & T > T^+ \end{cases} \tag{B.1}$$

in which $c_{p,LL} = 4000$ J/kg.K, $\Delta h_{pb} = 10^5$ J/kg, $T^+ = 310$, $T^- = 305$, $c_{p,GL} = 2000$ J/kg.K. The inlet temeratures of the heat exchanger are as follows; $T_{c,in} = 285$ and $T_{h,in} = 350$. Furthermore, the mass flow rate of the supercritical fluid is $m_c = 0.1$ kg/s. Furthermore, the perimeter is 0.145 m^2. The analytical solution for the temperature difference in the three different section of the heat exchanger can be written as;

$$T_h(x) - T_c(x) = \Delta T(x_i)\exp\left\{UP\left(\frac{1}{C_h} - \frac{1}{C_c}\right)x\right\}, \tag{B.2}$$

in which $\Delta T(x_i)$ is the temperature difference at location x_i. Note that location x_i denotes the locations $x = 0$, the location where $T = T^-$ and T^+ and finally $x = L$, where L is the length of the heat exchanger. Note that these four locations are easily determined while using Eq. (10). The temperature profile $T_h(x)$ can be determined per section with:

$$T_h(x) = T_h(x_i) + \left(\frac{1}{C_h} - \frac{1}{C_c}\right)^{-1}\left(\frac{1}{C_h}\right)\Delta T(x_i)\exp\left\{UP\left(\frac{1}{C_h} - \frac{1}{C_c}\right)x\right\} \tag{B.3}$$

The numerical method that was described earlier in Section 3 is used to obtain the temperature profiles for the aforementioned heat exchanger and is compared against the profiles that are described by Eqs. B.2 and B.3. Fig. B.15 shows that the numerical method is in excellent agreement with the analytical method.

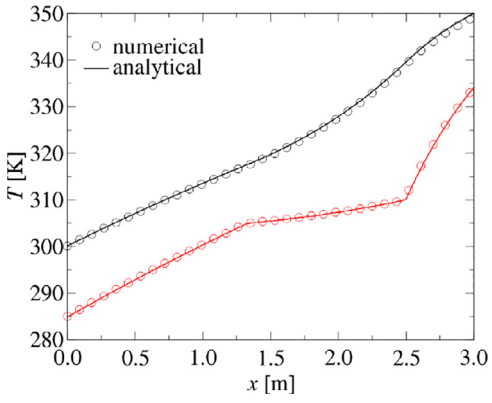

Fig. B.15. Comparison between the numerical method and the analytical method.

References

[1] D.T. Banuti, Crossing the widom-line – supercritical pseudo-boiling, J. Supercrit. Fluids 98 (2015) 12–16.
[2] A. Bejan, Entropy generation minimization, CRC Press, Inc., Boca Raton, Florida, U.S.A., 1996.
[3] A. Bruch, A. Bontemps, S. Colasson, Experimental investigation of heat transfer of supercritical carbon dioxide flowing in cooled vertical tube, Int J Heat Mass Transf 52 (2009). 2689–2598
[4] K. Brun, P. Friedman, R. Dennis, Fundamentals and applications of supercritical carbon dioxide (sco2) based power cycles, Woodhead Publishing an imprint of Elsevier, Duxford, United Kingdom, 2017.
[5] X. Chu, E. Laurien, Flow stratification co2 in a heated horizontal pipe, J Supercrit Fluids 116 (2016) 172–189.
[6] M.M. Ehsan, Z. Guan, A.Y. Klimenko, A comprehensive review on heat transfer and pressure drop characteristics and correlations with supercritical co2 under heating and cooling applications, Renwable and Sustainable Energy Reviews 92 (2018) 658–675.
[7] A. Fartaj, D.S.-K. Ting, W.W. Yang, Second law analysis of the transcritical co2 refrigeration cycle, Energy Convers. Manage. 45 (2004) 2269–2281.
[8] P. Forooghi, K. Hooman, Experimental analysis of heat transfer of supercritical fluids in plate heat exchangers, Int J Heat Mass Transf 74 (2014) 448–459.
[9] A.A. Gkountas, A.M. Stamatelos, A.I. Kalfas, Recuperators investigation for high temperature supercritical carbon dioxide power generation cycles, Appl Therm Eng 125 (2017) 1094–1102.
[10] V. Gnielinski, Neue gleichungen für den wärme- und den stoffübergang in turbulent durchströmten rohren und kanälen, Forsch. Ingenieurwes. 41 (1975) 8–16.
[11] J. Guo, Design analysis of supercritical carbon dioxide recuperator, Appl Energy 164 (2016) 21–27.
[12] P. Guo, S. Liu, J. Yan, J. Wang, Q. Zhang, Experimental study on heat trnasfer of supercritical co_2 flowing in a mini tube under heating conditions, Int J Heat Mass Transf 153 (2020) 119623.
[13] B. Halimi, K.Y. Suh, Computational analysis of supercritical co2 brayton cycle power conversion system for fusion reactor, Energy Convers. Manage. 63 (2012) 38–43.
[14] J. He, R. Tian, P. Jiang, S. He, Turbulence in a heated pipe at supercritical pressure, J Fluid Mech 920 (2021) A451–38.
[15] J. He, J. Yan, W. Wang, P. Jiang, S. He, Effects of buoyancy and thermophysical property variations on the flow supercritical carbon dioxide, International journal of heat fluid flow 86 (2020) 108697.
[16] J. Hesselgreaves, R. Law, D. Reay, Compact heat exchangers selection, design and operation, Butterworth-Heinemann, 2017.
[17] J.E. Hesselgreaves, Rationalisation of second law analysis of heat exchangers, Int J Heat Mass Transf 43 (2000) 4189–4204.
[18] B.D. Iverson, T.M. Conboy, J.J. Pasch, A.M. Kruizinga, Supercritical co_2 brayton cycles for solar-thermal energy, Appl Energy 111 (2013) 957–970.
[19] J. Jackson, Models of heat transfer to fluids at supercritical pressure with influences of buoyancy and acceleration, Appl Therm Eng 124 (2017) 1481–1491.
[20] J. Jackson, M.A. Cotton, B.P. Axcell, Studies of mixed convection in vertical tubes, Int. J. Heat Fluid Flow 10 (1989) 2–15.
[21] J. Jackson, W. Hall, Forced convection in channels and bundles, Hemisphere, vol. 2, New York, 1979.
[22] Y. Jiang, E. Liese, S.E. Zitney, D. Bhattacharyya, Design and dynamic modeling of printed circuit heat exchangers for supercritical carbon dioxide brayton cycles, Appl Energy 231 (2018) 1019–1032.
[23] Y. Jiang, E. Liese, S.E. Zitney, D. Bhattacharyya, Optimal design of microtube recuperators for an indirect supercrtical carbon dioxide recompression closed brayton cycle, Appl Energy 216 (2018) 634–648.
[24] F. Kauf, Determination of the optimum high pressure for transcritical co2-refrigeration cycles, Int. J. Therm. Sci. 38 (1999) 325–330.
[25] M. van der Kraan, M.M.W. Peeters, M.V.F. Cid, G.F. Woerlee, W.J.T. Veugelers, G.J. Witkamp, The influence of variable phyiscal properties and buoyancy on heat exchanger design for near- and supercritical conditions, J Supercrit Fluids 34 (2005) 99–105.
[26] E.A. Krasnoshchekov, V.S. Protopopov, V. Fen, I.V. Kraeva, Experimental investigation of heat transfer for carbon dioxide in the supercritical region, In: Gazley, Jr., C., Hartnett, J.P., Ecker, E.R.C. (Eds.), Proceedings of the Second All-Soviet Union Conference on Heat and Mass Transfer, Minsk, Belarus, May, 1964, Published as Rand Report R-451-PR 1 (1967) 26–35.
[27] A. Kruizinga, M. Anderson, R. Fatima, M. Corradini, A. Towne, D. Ranjan, Heat transfer of supercritical carbon diozide in printed circuit heat exchanger geometries, J Therm Sci Eng Appl 3 (2011) 031002.
[28] V.A. Kurganov, Y.A. Zeigarnik, I.V. Maslakova, Heat transfer and hydraulic resistance of supercritial-pressure coolants. part i: specifics of thermophysical properties of supercritical pressure fluids and turbulent heat transfer under heating conditions in round tubes (state of the art), Int J Heat Mass Transf 55 (2012) 3061–3075.
[29] J.S. Kwon, S.J. Bae, J.Y. Heo, J.I. Lee, Development of accelearted pche off-design performance model for optimizing power system operation strategies in s-co_2 brayton cycle, Appl Therm Eng 159 (2019) 113845.
[30] J.S. Kwon, S.S. andd J. Y. Heo, J.I. Lee, Compact heat exchangers for supercritical co_2 power cycle application, Energy Convers. Manage. 209 (2020) 112666.
[31] H. Li, Y. Zhang, L. Zhang, M. Yao, A. Kruizinga, M. Anderson, Pdf-based modeling on the turbulent convection heat transfer of supercritical co_2 in the printed circuit heat exchangers for the supercritical co_2 brayton cycle, Int J Heat Mass Transf 98 (2016) 204–218.
[32] S.M. Liao, T.S. Zhao, A. Jakobsen, A correlation of optimal heat rejection pressures in transcritical carbon dioxide cyles, Appl Therm Eng 20 (2000) 831–841.
[33] G. Liu, Y. Hunag, J. Wang, R. Liu, A review on the thermal-hydraulic performance and optimization of printed circuit heat exchangers for supercritical co2 in advanced nuclear power systems, Renewable Sustainable Energy Rev. 153 (2020) 110290.
[34] Y. Liu, Y. Wang, D. Huang, Supercritical co_2 brayton cycle: astate-of-the-art review, Energy 189 (2019) 115900.
[35] W.L. Luyben, Heat exchanger simulations involving phase changes, Comput. Chem. Eng. 67 (2014) 133–136.
[36] K. Manjunath, S.C. Kaushik, Second law thermodynamic study of heat exchangers: areview, Renewable Sustainable Energy Rev. 40 (2014) 348–374.
[37] M. Marchionni, G. Bianchi, S.A. Tassou, Techno-economic assessment of joule-brayton cycle architecture for heat to power conversion from high-grade heat sources using co2 in the supercritical state, Energy 148 (2018) 1140–1152.
[38] F. Maxim, K. Karalis, P. Boillat, D.T. Banuti, J.I.M. Damian, B. Niceno, C. Ludwig, Thermodynamics and dynamics of supercritical water pseudo-boiling, Adv. Sci. (2020) 2002312.
[39] M. Mecheri, Y.L. Moullec, Supercritical co2 brayton cycles for coal-fired power plants, Energy 103 (2016) 758–771.
[40] H. Nemati, A. Patel, B.J. Boersma, R. Pecnik, Mean statistics of a heated turbulent pipe flow at supercritical pressure, Int J Heat Mass Transf 83 (2015) 741–752.
[41] K. Nikitin, Y. Kato, L. Ngo, Printed circuit heat exchanger thermal-hydraulic performance in supercritical co_2 experimental loop, Int. J. Refrig 29 (2006) 807–814.
[42] J.W.R Peeters, R. Pecnik, M. Rohde, T. van der Hagen, B. Boersma, Turbulence attenuation in simultaneously heated and cooled annular flows at supercritical pressure, J Fluid Mech 799 (2016) 505–540.
[43] J.W.R. Peeters, R. Pecnik, M. Rohde, T. van der Hagen, B. Boersma, Characteristics of turbulent heat transfer in an annulus at supercritical pressure, Phys. Rev. Fluids 2 (2017) 024602.
[44] J.W.R. Peeters, M. Rohde, A heat transfer - friction analogy for fluids at supercritical pressure, J Supercrit Fluids 150 (2019) 75–85.
[45] B. Petukhov, A. Polyakov, Heat transfer in turbulent mixed convection, Springer, 1988.
[46] I.L. Pioro, H.F. Khartabil, R.B. Duffey, Heat transfer to supercritical fluids flowing in channels – empircal correlations (survey), Nucl. Eng. Des. 230 (2004) 69–91.
[47] J. Ren, O. Marxen, R. Pecnik, Boundary-layer stability of supercritical fluids in the vicinity of the widom line, J Fluid Mech 871 (2019) 831–864.
[48] W. Roetzel, X. Luo, D. Chen, Design and operation of heat exchangers and their networks, Academic Press, 2020.
[49] E. Ruiz-Casanova, C. Rubio-Maya, J.J. Pacheco-Ibarra, V.M. Ambriz-Díaz, C.E. Romero, X. Wang, Thermodynamic analysis and optimization of supercritical carbon dioxide brayton cycles for use with low-grade geothermal heat sources, Energy Convers. Manage. 216 (2020) 112978.
[50] M. Saeed, A.S. Berrouk, M.S. Siddiqui, A.A. Awais, Effect of printed circuit heat echanger's different designs on the performance of supercritical carbon dioxide brayton cycle, Appl Therm Eng 179 (2020) 115758.
[51] M. Saeed, S. Khatoon, M.-H. Kim, Design optimization and performance analysis of a supercritical carbon dioxide recompression brayton cycle based on the detailed models of the cycle components, Energy Convers. Manage. 196 (2019) 242–260.
[52] J. Sarkar, Second law analysis of supercritical co2 recompression brayton cycle, Energy 34 (2009) 1172–1178.
[53] J. Sarkar, S. Bhattacharyya, M.R. Gopal, Optimization of a transcritical co2 heat pump cycle for simultaneous cooling and heating applications, Int. J. Refrig 27 (2004) 830–838.
[54] S.I. Schöffer, S.A. Klein, P.V. Aravind, R. Pecnik, A solid oxide fuek cell- supercritical carbon dioxide brayton cycle hybrid system, Appl Energy 283 (2021) 115748.
[55] A. Sciacovelli, V. Verda, E. Sciubba, Entropy generation analysis as a design tool – a review, Renewable Sustainable Energy Rev. 43 (2015) 1167–1181.
[56] D.P. Sekulić, Entropy generation in a heat exchanger, Heat Transfer Eng. 7 (1986) 83–88.
[57] Y. Song, F. Cao, The evaluation of optimal discharge pressure in a water-precooler-based transcritical co2 heat pump system, Appl Therm Eng 131 (2018) 8–18.
[58] D. Sánchez, J. Patiño, C. Sanz-Kock, R. Llopis, R. Cabello, E. Torella, Energetic evaluation of a co2 refrigeration plant working in supercritical and subcritial conditions, Appl Therm Eng 66 (2014) 227–238.
[59] K. Wang, Y.-L. He, Thermodynamic analysis and optimization of a molten salt solar power tower integrated with a recompression supercritical co2 brayton cycle based on integrated modeling, Energy Convers. Manage. 135 (2017) 336–350.
[60] S. Wright, R. Radel, M. Vernon, G. Rochau, P. Pickard, Operation and Anlysis of a Supercritical CO2 Brayton Cycle, Technical Report, Sandia National Laboratories, Albuquerque, New Mexico 87185 and Livermore, California 94550, 2010.
[61] K. Yamagata, K. Nishikawa, S. Hasegawa, T. Fujii, S. Yoshida, Forced convective-heat transfer to supercritical water flowing in tubes, Int J Heat Mass Transf 15 (1972) 2575–2593.
[62] J.Y. Yoo, The turbulent flows of supercritical fluids with heat transfer, Annual reviews of fluid mechanics 45 (2013) 495–525.

[63] L.-Z. Zhang, Conjugate heat and mass transfer in heat mass exchanger ducts, Academic Press, 2014.
[64] X.P. Zhang, X.W. Fan, F.K. Wang, H.G. Shen, Theoretical and exerimental studies on optimum heat rejection pressure for a co2 heat pump system, Appl Therm Eng 30 (2010) 2537–2544.
[65] Y. Zhang, Y. Yao, Z. Li, G. Tang, Y. Wu, H. Wang, J. Lu, Low-grade heat utilization by supercritical carbon dioxide rankine cycle: analysis on the performance of gas heater subjected to heat flux and convective boundary conditions, Energy Convers. Manage. 162 (2018) 39–54.